Journal of the European Ceramic Society **8** (1991) 47–57

Description and Role in High-temperature Deformation of Grain Boundaries in α-Alumina Ceramics

L. Priester & S. Lartigue

Laboratoire de Métallurgie Structurale, Unité Associée au CNRS n° 1107, Bât. 413, Université Paris Sud, 91405 Orsay Cédex, France

(Received 15 December 1990; revised version received 20 February 1991; accepted 6 March 1991)

Abstract

This paper strives to assess the importance of grain boundaries in a polycrystal by giving a typical example of theoretical and experimental approaches in the case of thermomechanical aluminas, this oxide being considered as the paradigm of the non-cubic ceramics. Grain boundary diffusion limited grain boundary sliding is the prevailing deformation process at high temperature. In this work, the micromechanisms involved in grain boundary sliding are revealed by transmission electron microscopy; furthermore, the results point out important differences in the contribution of grain boundaries to the overall deformation according to their crystallographic parameters. This relationship between geometry and behavior has been investigated on the basis of a theoretical description of grain boundaries established for rhombohedral lattices.

Diese Arbeit befaßt sich mit der Bedeutung der Korngrenzen in polykristallinen Materialien und zeigt anhand eines typischen Beispiels ihre theoretische und experimentelle Beschreibung in thermomechanischer Hinsicht für Al_2O_3 auf. Dieses Oxid stellt das Musterbeispiel der nichtkubischen keramischen Werkstoffe dar. Durch Korngrenzendiffusion kontrolliertes Korngrenzengleiten stellt bei hohen Temperaturen den vorherrschenden Verformungsmechanismus dar. Mittels TEM wird die Mikromechanik dieser Korngrenzengleitung aufgezeigt. Darüberhinaus zeigen die Ergebnisse eine deutliche Abhängigkeit des Beitrags der Korngrenzen zur Gesamtverformung von ihren kristallographischen Parametern. Dieser Zusammenhang zwischen Geometrie und Verhalten wurde auf der Basis einer theoretischen Betrachtung von Korngrenzen mit rhomboedrischem Gitter untersucht.

On a étudié l'importance des joints de grains dans un polycristal en donnant un exemple typique d'approche théorique et expérimentale dans des alumines thermomécaniques, cet oxyde pouvant être considéré comme un modèle pour les céramiques non cubiques. Le déplacement des joints de grain limité par la diffusion aux joints de grains est le mécanisme de déformation qui prévaut à haute température. Dans cette étude, les micromécanismes mis en jeu dans le déplacement des joints de grains sont révélés par microscopie électronique à transmission; les résultats obtenus montrent, en outre, des différences importantes au niveau de la contribution des joints de grains à la déformation générale selon leurs paramètres cristallographiques. Cette relation entre la géométrie et le comportement a été étudiée sur la base d'une description théorique des joints de grains établie pour les réseaux rhomboédriques.

1 Introduction

Fine-grained alumina polycrystals doped with magnesia alone or with magnesia plus yttria display a high ductility under high-temperature compression.[1,2] This behavior may be seen as a structural superplasticity, always associated with a very small grain size. This requirement strongly suggests an important contribution of grain boundary phenomena in the deformation processes.

The main purpose of the present work is to understand the role of the grain boundary structure in grain boundary sliding micromechanisms, which has not been thoroughly investigated until now, especially in the case of ceramics.

As a prequisite to the experimental study, a fundamental description of grain boundaries in

Journal of the European Ceramic Society 0955-2219/91/$3.50

Al_2O_3 is presented. The geometric approach developed by Bollmann,[3] extensively used for cubic materials and for metallic systems, is extended to rhombohedral lattices and tested, in order to assess its relevance to the description of grain boundaries in an ionic oxide. Indeed, this purely geometric model does not take into account the content of the cell, thus differences between the possible Burgers vectors of the grain boundary dislocations derived from the model and the effective Burgers vectors may be expected. Finally, the fundamental study consists in a 'to and fro' movement between theory and transmission electron microscopy (TEM) experiments to make sure of the validity of the geometric tool for describing Al_2O_3 grain boundaries and then, to undertake a possible applied study.

The applied study intends to relate microscopic analyses to macroscopic behaviors and thus requires a great number of investigations, which are interpreted on the basis of the geometric tool previously established. This study necessarily implies two steps:

—First, the role of grain boundaries in the deformation process must be emphasized. In particular, the possibility that this role differs according to the grain boundary structure is still an open question. It leads to the determination of possible relationships between specific grain misorientation or specific grain boundary plane orientation and specific grain boundary behavior under deformation. Provided that such relationships may be established, these 'specific grain boundaries' may be classified as 'special' because their geometrical speciality is linked to a special property.

—Then, in order to analyze the grain boundary contribution to the overall property of the material, the distributions in the polycrystal of the grain boundaries according to their geometry must be determined, hereafter referred to as 'grain misorientation texture' and 'grain boundary plane texture'.

2 Theoretical Coincidences for Grain Boundaries in Rhombohedral Alumina

For a good understanding of the theoretical approach to coincidences in the case of rhombohedral lattices, reference should be made to the work of Grimmer;[4-6] only brief explanations are given in this section.

In the case of cubic symmetry a coincidence lattice is always obtained by rotation of one crystal with respect to another, the rotation matrix **R** being always rational. However, in the case of trigonal symmetry, **R** is a function of the c/a ratio, which is generally an irrational number for real materials. Then, a multiple common cell may be defined if, and only if, the rotation matrix, expressed in rhombohedral coordinates, is rational. As a consequence, two kinds of exact coincidences may be considered:

(i) Common exact coincidences (common to all rhombohedral lattices) are obtained by common rotations independent of the c/a ratio.

(ii) Rational (exact) coincidences occur for specific rotations (**R** is rational) that may be only found for specific values of c/a, such that $(c/a)^2$ is rational. From a practical point of view, rational coincidences are unlikely to occur because the real c/a ratio generally differs from any specific c/a value. In this case, specific rotations do not generate exact coincidences but only lead to near coincidences between the two lattices. In other words, rotation is not sufficient to superimpose a multiple cell of crystal (1) and a multiple cell of crystal (2). Therefore, the exact rational coincidences may only serve as references for the description of real grain boundaries.

2.1 Common rotations/exact coincidences for rhombohedral lattices

Exact coincidences between two rhombohedral lattices derive from rotations around the [0001] c axis with θ angles, such that $\sqrt{3}\tan(\theta/2)$ is rational (equivalent 180° rotations around axes perpendicular to [0001] exist). By limiting Σ to 36°, only six exact coincidences are obtained; among them the basal twin (Σ 3, 60° [0001]) leaves the oxygen ions unchanged. (Ordered grain boundaries have been found for higher Σ values in cubic metals but, generally, most coincidence boundaries in real polycrystals present relatively low Σ values;[7] moreover, the extension of the coincidence calculation to $\Sigma = 50$ in the case of alumina does not lead to significant changes.)

2.2 Specific rotations/near coincidences for rhombohedral alumina

Specific rotations have been determined by using two alternative techniques.

(i) The rotation matrices have been calculated by choosing different rational values of $(c/a)^2$

Table 1. Rational values of c^2/a^2 that surround the real value for alumina ($c^2/a^2 = 231/31$) and give rise to rational coincidences with $\Sigma \leq 36$

c^2/a^2	c/a	c^2/a^2	c/a
51/7 = 7·286	2·699	231/31 = 7·452	2·730
117/16 = 7·313	2·704	15/2 = 7·5	2·739
22/3 = 7·333	2·708	483/64 = 7·547	2·747
147/20 = 7·35	2·711	219/29 = 7·552	2·748
96/13 = 7·385	2·717	174/23 = 7·565	2·750
237/32 = 7·406	2·721	129/17 = 7·588	2·755
141/19 = 7·421	2·724	213/28 = 7·607	2·758
186/25 = 7·44	2·728	84/11 = 7·636	2·763

that surround the real value $[(c/a)^2_{Al_2O_3} = 7{\cdot}452]$ (Table 1).[8]

(ii) The second method[9] starts with the real c/a ratio and computes step by step two multiple cells M_1 and M_2 of the two crystals very close in shape and size such that:

$$M_1 \xrightarrow{\mathbf{A}=\mathbf{RD}} M_2$$

the transformation **A** being the product of a deformation **D** by a rotation **R**.

A specific rotation is obtained when M_1 may be transformed into M_2 by a pure deformation:

$$M_1 \xrightarrow{\mathbf{A}=\mathbf{D}} M_2$$

In the case of a rhombohedral lattice

$$\mathbf{D} = \begin{bmatrix} -e & 0 & 0 \\ 0 & 0 & 0 \\ 0 & 0 & e \end{bmatrix}$$

In principle there is no reason why the specific rotations obtained by the two methods should coincide, but, in fact, the differences may be neglected:

$$\Delta\mathbf{R} = \mathbf{R}_{(1)} \cdot \mathbf{R}^{-1}_{(2)} \leq 0{\cdot}01^\circ$$

Coincidence tables for the various c/a ratios (Table 1) have been established using the first method. The number of rational coincidences ($\Sigma \leq 36$) differs strongly from one c/a value to another. In particular, the maximum number (30) is obtained for $c^2/a^2 = 15/2$; c^2 and a^2, being two integers without a common divisor, have, in that case, the smallest values and $(c/a)_{sp}$ differs from $(c/a)_{exp}$ by 0·009. In contrast, for the nearest specific c/a from the real c/a (equal to 2·730) only one coincidence ($\Sigma = 36$) has been found.

The second method allows the determination of the deformation e which is required to describe the grain boundary structure in terms of dislocations. Indeed, intrinsic grain boundary dislocations must originate from the total misfit between the two crystals $\mathbf{A} = \mathbf{RD}$ (**R** is the experimental rotation which most often differs from any specific rotation). Then, the grain boundary dislocation content is given by an extended Bollmann equation:

$$(\mathbf{I} - \mathbf{A}^{-1})\mathbf{x}_c = \mathbf{b}_1$$

with $\mathbf{A} = \mathbf{RD}$; $\mathbf{I}$ = unit matrix; $\mathbf{x}_c$ denotes translation vectors giving all the best matching points of the two lattices called 'c-points' (equivalent to the O-points in the Bollmann approach); $\mathbf{b}_1$ are the possible Burgers vectors of the intergranular dislocations expressed in the coordinates of crystal 1.

Table 2. Possible near-coincidence descriptions of a rhombohedral twin according to the choice of the specific c/a ratio ($(c/a)_{exp} \simeq 2{\cdot}73$)

a/c	*Misorientation*		Σ	ε ($\times 10^{-3}$)
	Angle	*Axis*		
2·699	86·42	[0 2 $\bar{2}$ 1]	8	8
2·708	86·30	[0 2 $\bar{2}$ 1]	31	7
2·711	86·26	[0 2 $\bar{2}$ 1]	23	6
2·717	86·18	[0 2 $\bar{2}$ 1]	15	4
2·724	86·09	[0 2 $\bar{2}$ 1]	22	2
2·728	86·05	[0 2 $\bar{2}$ 1]	29	1
2·730	86·02	[0 2 $\bar{2}$ 1]	36	0
2·739	85·90	[0 2 $\bar{2}$ 1]	7	3
2·748	85·78	[0 2 $\bar{2}$ 1]	34	6
2·750	85·75	[0 2 $\bar{2}$ 1]	27	7
2·755	85·70	[0 2 $\bar{2}$ 1]	20	8
2·758	85·66	[0 2 $\bar{2}$ 1]	33	9
2·763	85·59	[0 2 $\bar{2}$ 1]	13	11

The consideration of the coincidence tables given elsewhere[7] raises two closely related questions:

(i) Is the use of a particular coincidence table, corresponding to a particular rational c/a value, more relevant to the classification of grain boundaries in alumina polycrystals? That is, to select, by reference to these coincidences only, those grain boundaries that are likely to display special behavior. In this form, the question deals with a statistical and practical point of view.

(ii) Insofar as thorough analyses of some grain boundary structures are needed, the previous problem must be faced in another way. The same grain boundary may be described by reference to different couples (Σ, ε) appearing in the different coincidence tables. For example, the plurality of the possible descriptions of the rhombohedral twin is shown in Table 2; for different very close θ angles ($\Delta\theta < 1^\circ$) around the same [0 2 $\bar{2}$ 1] axis, 13 descriptions, and thus theoretically 13 associated grain boundary structures, are possible.

Is there a description which better fits with the observed grain boundary, i.e. which accounts for its dislocation content? The underlying reason of this question is energy minimization.

The next section, as a point of the fundamental approach, deals with the two aspects, 'qualitative' and 'quantitative', of this important question.

3 Experimental Near-coincidence Grain Boundaries in Alumina

In order to assess the ability of the theoretical model to describe real near-coincidence grain boundaries, the first step consists of 'recognizing' these grain boundaries in a polycrystal and comparing, for each of them, the experimental misorientation determined by TEM for the neighboring misorientations associated with different theoretical coincidences.

The basic assumption was the following: the occurrence in a grain boundary of a strictly periodic network of intrinsic dislocations or a pseudo-periodic network of extrinsic dislocations is a criterion for assuming that this grain boundary is a near-coincidence one, a crystalline structure being preserved in the interface.[10] The maximum allowed deviation $\Delta\theta_c$ between the experimental misorientation θ_{exp} and the theoretical misorientation θ_{th} (common or specific) has been chosen in agreement with the Brandon criterion, extensively used for cubic and metallic systems:[11]

$$\Delta\theta_{exp} = |\theta_{th} - \theta_{exp}|$$
$$\Delta\theta_{exp} \leq \Delta\theta_c = 15^\circ\, \Sigma^{-1/2}$$

3.1 Statistical study of grain boundaries

About 300 grain boundaries have been investigated in various aluminas, 57 presenting dislocation networks. Among them, there are few low-angle grain boundaries (near $\Sigma = 1$) and only two are close to the $\Sigma = 3$ exact coincidence (basal twin); 25 grain boundaries have been interpreted on the basis of a 'one-dimensional coincidence' model (ODC) well-known previously under the name of 'plane matching';[12] this model corresponds to a good matching of dense planes of alumina across the grain boundary plane.[13]

Finally, 18 grain boundaries may be described as three-dimensional near-coincidence grain boundaries provided reference is made to the coincidence table corresponding to $c^2/a^2 = 15/2$ (see Section 2.2). Among these grain boundaries, four of them are such that $\Sigma = 3\Sigma'$, where Σ' may be seen as the coincidence index for the oxygen sub-lattice. It must be noted that no grain boundary plane is a symmetry plane of the structure.

If any of the fifteen other tables (other $(c/a)_{sp}$) is chosen as reference, most of the previous grain boundaries would escape coincidence relationship, although they contain dislocation networks.

Thus, the table established for $(c/a)^2 = 7{\cdot}5$, including the maximum number of coincidences with $\Sigma \leq 36$ and corresponding to the smallest Σ values with reasonable ε values ($\varepsilon \cong 10^{-3}$), appears more appropriate to account for periodic dislocation occurrence in alumina grain boundaries.

This remark does not necessarily imply that, for any grain boundary, the same table may be used to predict the intrinsic dislocation characteristics (line orientation and Burgers vector).

3.2 Analysis of near $\Sigma = 7$ grain boundary dislocations

First, the basic vectors, $\mathbf{b}_1$, $\mathbf{b}_2$, $\mathbf{b}_3$ of the DSC (displacement shift complete) lattices associated with the rational coincidence descriptions of a rhombohedral twin ($\Sigma = 7$) (see Table 2) have been calculated. These vectors give the allowed Burgers vectors of the grain boundary dislocations. As Σ increases, the magnitude of $\mathbf{b}_1$ strongly decreases, while, in contrast, $\mathbf{b}_2$ and $\mathbf{b}_3$ preserve almost the same direction and magnitude.[8] By considering that the Burgers vector of an intrinsic dislocation is at most equal to $\mathbf{b}_L$ (L for lattice) and by choosing the prismatic dislocation $\mathbf{b}_p$ as lattice dislocation ($|\mathbf{b}_p| = 0{\cdot}824$ nm,[14] the various linear combinations of $\mathbf{b}_1$, $\mathbf{b}_2$ and $\mathbf{b}_3$ lead to a huge number (>200) of possible Burgers vectors. Phenomena of dissociation may also be expected. Therefore, determination of actual Burgers vectors is not straightforward.

The observed near-coincidence grain boundary presents a rotational deviation from the rhombohedral twin misorientation of 0·4° around an axis inclined to the grain boundary plane with an angle of 20°; it has mostly a tilt character.

Two families of dislocations may be observed, at least (Fig. 1(a)):

—A first network (C) composed of regularly spaced dislocations with a narrow contrast.
—The dislocations of the second family (B) disturb the periodicity of the previous one and their contrast is stronger.
—The micrograph (Fig. 1(b)), obtained with a common diffraction vector, clearly reveals a lattice dislocation which impinges on the grain boundary (in X) and emerges in a pore at its

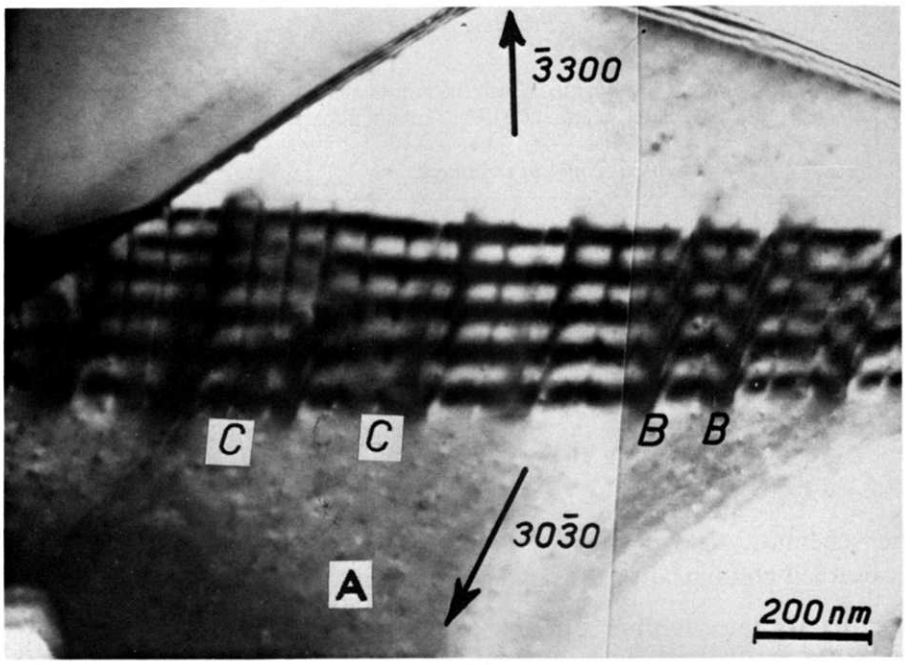

(a)

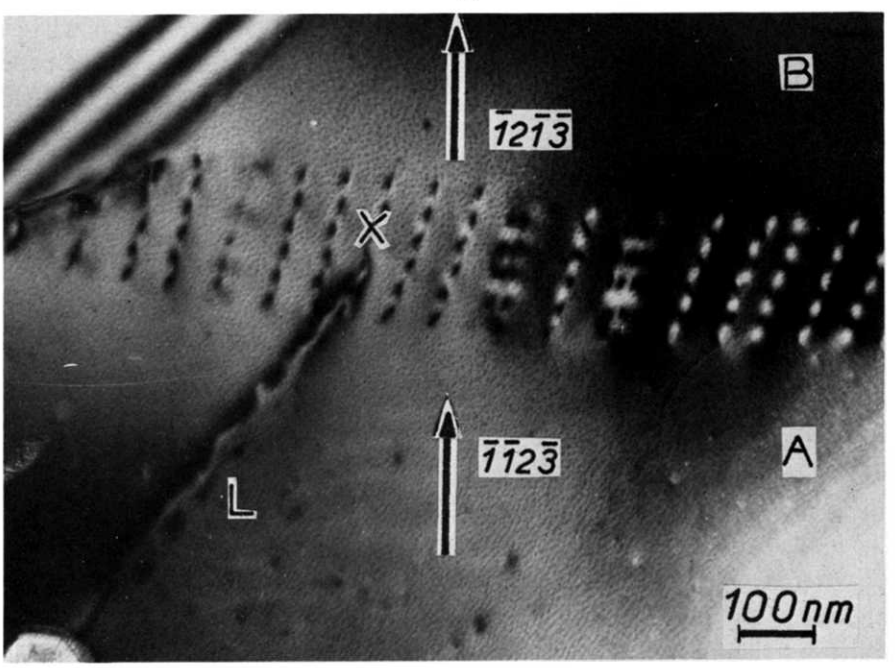

(b)

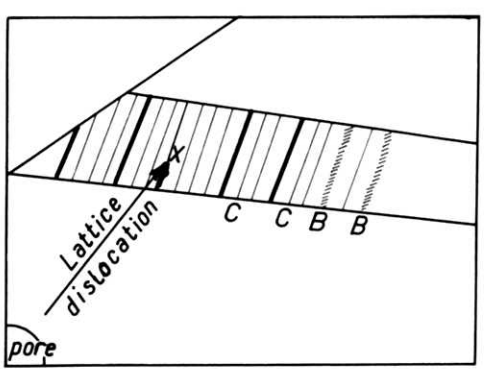

(c)

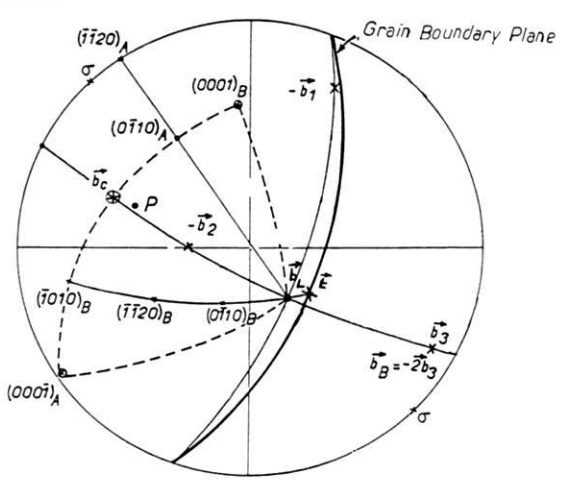

(d)

Fig. 1. Intergranular dislocations in a near $\Sigma = 7$ boundary (rhombohedral twin): intrinsic network of dislocations (C) and extrinsic dislocations (B) are clearly visible in (a) a simultaneous two-beam condition micrograph; (b) a lattice dislocation enters the grain boundary in X; (c) the configuration is represented on the scheme; (d) the stereographic projection of the two grains showing their relative orientation, the grain boundary plane and the Burgers vectors of the different dislocations.

Table 3. The different kinds of Al_2O_3 samples investigated (from the points of view of purity and thermomechanical treatments) and the associated characteristics of intergranular dislocations

Materials	*Thermomechanical treatments*	*Intergranular dislocations*
Pure Al_2O_3 (undoped)	Hot-pressed[a]	Few periodic networks of intrinsic dislocations
Al_2O_3 + 500 ppm MgO	Hot-pressed[a]	Some periodic networks + few aperiodic networks
	Hot-pressed[a] + stress-free annealed (1500°C)	
	Hot-pressed[a] + deformed[b]	Numerous pseudo-periodic networks of extrinsic dislocations
Al_2O_3 + 500 ppm MgO + 500 ppm Y_2O_3	Hot-pressed[a]	
	Hot-pressed[a] + deformed[b]	

[a] 1500°C, 45 MPa.
[b] 1500°C, 30 MPa, $\varepsilon = -0{\cdot}27$.

other end. The schematic drawing (Fig. 1(c)) illustrates the observed configuration.

After a first selection of the possible Burgers vectors by a semiquantitative contrast analysis, the determination of **b** is achieved by comparison of computed and experimental dislocation images (Fig. 1(d)):[13]

$$\mathbf{b}_C = -(\mathbf{b}_2 + \mathbf{b}_3) \cong \tfrac{1}{7}[0\ \bar{5}\ 5\ \bar{2}]$$
$$\mathbf{b}_B = 2\,\mathbf{b}_3 = \tfrac{2}{21}[\bar{7}\ 4\ 11\ \bar{3}]$$
$$\mathbf{b}_L = \mathbf{b}(\text{basal}) = \tfrac{1}{3}[\bar{2}\ 1\ 1\ 0]$$

These results perfectly fit with the following reaction:

$$\mathbf{b}_L + \mathbf{b}_C \rightarrow \mathbf{b}_B$$

in which dislocations C and B are intrinsic and extrinsic dislocations respectively. But they do not allow any conclusion to be made about the best among the grain boundary descriptions associated with the specific c/a values close to the real c/a $[(\Delta c/a)/(c/a) \leq 10^{-2}]$. As a matter of fact, $\mathbf{b}_C$ and $\mathbf{b}_B$ are linear combinations of $\mathbf{b}_2$ and $\mathbf{b}_3$, which are almost identical whatever the description of the rhombohedral twin.

This ambiguity might be solved by determination of the dislocation line direction and comparison with the calculated O-line in the grain boundary plane[3,15] or by analysis of a $\mathbf{b}_1$ dislocation; this DSC vector, very small compared to $\mathbf{b}_2$ and $\mathbf{b}_3$, changes with Σ. The high-resolution electron microscopy (HREM) observation of a rhombohedral twin made some years ago in haematite, F_3O_4[16] (this oxide possesses a cell isostructural to that of alumina), may be interpreted in that way. A Frank circuit around the twin reveals a closure failure of 0·077 nm: this value equals the $|\mathbf{b}_1|$ Burgers vector corresponding to $\Sigma = 7$ and thus to the specific c/a value = 2·739 $(c^2/a^2) = 7{\cdot}5$).

This interpretation and others about hexagonal materials[17] support the conclusion of the 'statistical' study of alumina concerning the choice of a more appropriate coincidence table (see Section 3.1). Near-coincidence grain boundaries seem to adopt the structure corresponding to the smallest Σ value, even though it does not lead to the smallest deformation. It is not clear why this should give rise to the smallest energy. More experimental observations, taking into account the grain boundary plane and the grain boundary chemistry, are required to fully assess the occurrence of a preferred structure for a given grain boundary.

When performing an extended applied study (Sections 4 and 5), the use of the coincidence table established for $c^2/a^2 = 7{\cdot}5$ appears satisfactory for the characterization of the three-dimensional near-coincidence grain boundaries in alumina polycrystals; intrinsic dislocations may or may not be revealed by TEM in these grain boundaries.

4 Geometrical 'Speciality' and 'Special' Behavior of Grain Boundaries under Deformation

4.1 Preliminary

Six kinds of alumina samples have been studied (Table 3).

Pure alumina displays a large grain size microstructure after sintering.[18] Several grains are elongated and bordered with straight interfaces which are dense planes of the structure, most often the basal plane (Fig. 2). These planes are faceted, alternately (0001) in one grain and then in the other grain (Fig. 3).

Doping with MgO leads to small grain sizes of less than 1 μm (Fig. 4). The average grain size is reduced again by codoping with Y_2O_3.

Pure and doped aluminas differ strongly from the point of view of their ductility. Pure Al_2O_3 cannot be deformed, even at high temperature, while doped and codoped Al_2O_3 polycrystals are very ductile under compression.

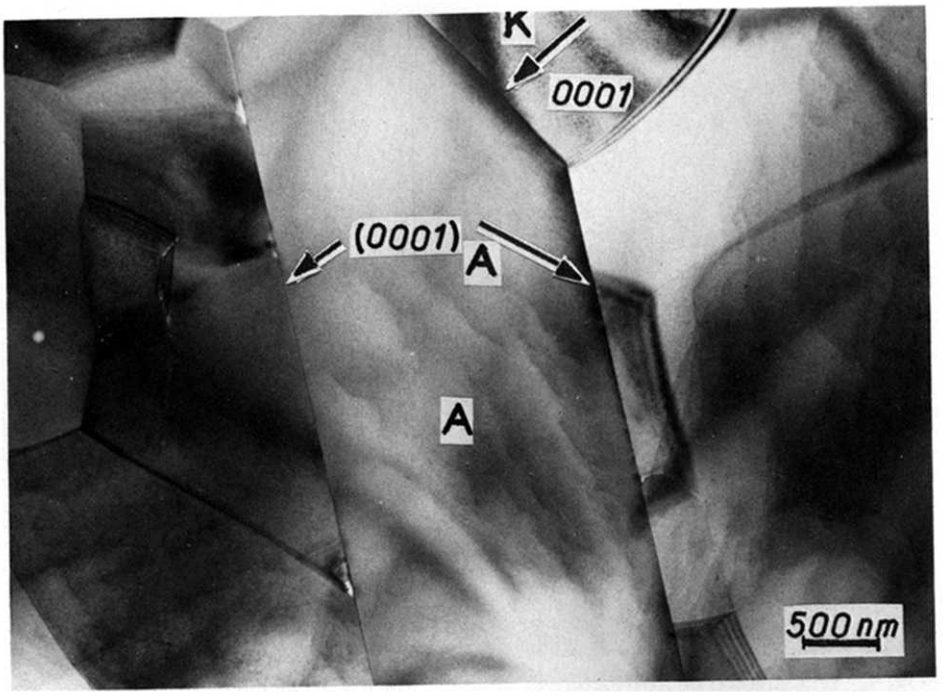

Fig. 2. Large and elongated grains characterize the microstructure of pure alumina after sintering.

The constitutive law is:[1,19]

$$\dot{\varepsilon} = \frac{\sigma^{1.4}}{d^3}$$

The cubic exponent of the grain size d indicates that most probably grain boundary diffusion is operating (Coble mechanism); but the process is not a pure diffusion, the stress exponent being different from the unit (between 1 and 2). Codoping with yttrium leads to a decrease of the strain rate.

4.2 Grain boundary geometry and intergranular dislocations

The distributions and the characteristics of grain boundary dislocations are very sensitive to the purity of the samples and to the thermomechanical treatments they underwent (Table 3). Isolated extrinsic dislocations were never observed. Very few periodic networks of intrinsic dislocations were found in pure alumina. Their number is appreciably higher in hot-pressed and annealed aluminas

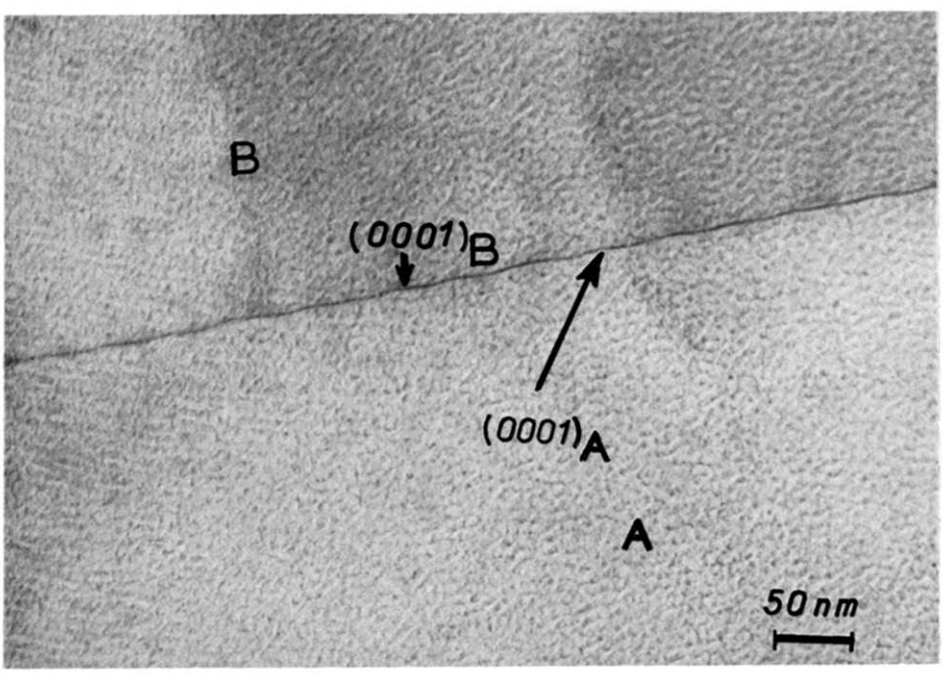

Fig. 3. Observed with higher magnification, straight grain boundaries of Fig. 2 appear faceted.

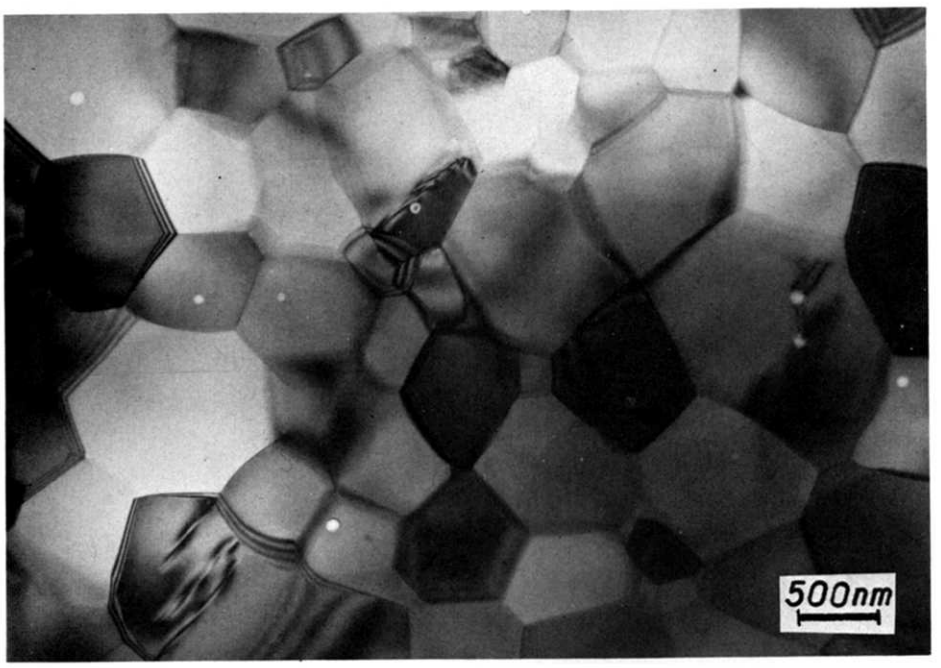

Fig. 4. Fine-grained microstructure of alumina doped with magnesia after sintering.

doped with MgO; simultaneously some extrinsic dislocations appear in the form of pseudo-periodic arrangements. The occurrence of the latter phenomenon strongly increases in deformed doped and codoped aluminas, and directly after hot-pressing in the presence of yttria. These aperiodic networks are generally found in near-coincidence grain boundaries; only very few of them appear in general grain boundaries, always adjacent in that case to near-coincidence grain boundaries containing extrinsic dislocations.

The occurrence of a pseudo-periodic network of extrinsic dislocations indicates that grain boundaries are in a relaxed non-equilibrium state.[10] In the case of alumina, it results from high-temperature deformation and is favored by yttrium; this element has been found strongly segregated to gain boundaries by STEM analyses.

Thorough observations of these networks point out several features that may be related to the deformation processes:

(i) Aperiodic networks are always located in contiguous grain boundaries in some regions of the polycrystal (Fig. 5). The dislocations present a curve profile in favor of their motion in the grain boundary.[20] They may form pile-ups at triple points or in the vicinity of a grain boundary ledge.

These remarks suggest that grain boundary sliding may occur by accommodation of extrinsic dislocations which leads to their arrangement in pseudo-periodic networks in 'special' grain boundaries (low-angle, one-dimensional and near-rational coincidences) and their disappearance in general grain boundaries.[10] Complete accommodation cannot be realized in 'special' grain boundaries and sliding is impeded. Stress relaxations are more easy in general grain boundaries for two reasons: spreading (or dissociation) of extrinsic dislocations may occur and their displacement from one general grain boundary to another one is not inhibited. In contrast, the junction between two special grain boundaries may be submitted to stress concentrations (pile-ups), the relaxation of which leads to cavitation.[21]

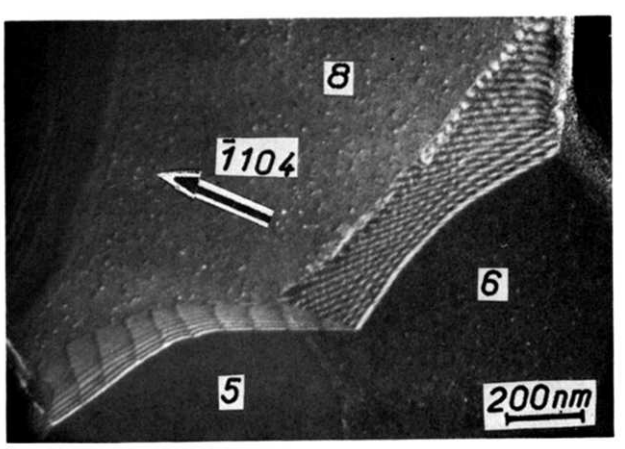

Fig. 5. Weak-beam TEM micrograph showing grain boundary dislocation networks in a deformed Mg-doped alumina sample: two networks (intrinsic and probably extrinsic) are visible in a near $\Sigma = 19$ grain boundary (6/8); the curved dislocations irregularly spaced in the one-dimensional coincidence boundary (5/8) are unambiguously extrinsic.

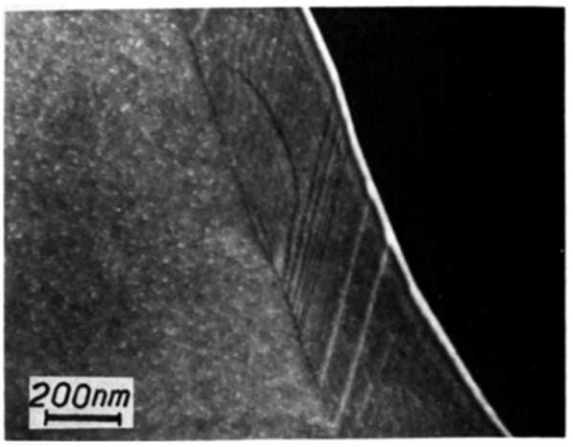

Fig. 6. Extrinsic dislocations seem to be generated within the grain boundary in a deformed sample of alumina doped with magnesia and yttria.

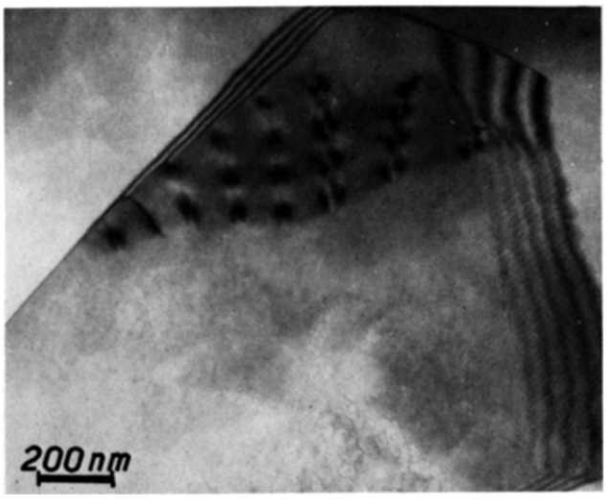

Fig. 7. Lattice dislocations impinge on and do not enter a special grain boundary in Mg-doped alumina co-doped with yttria.

These different sliding behaviors of general and special grain boundaries have already been found in various metallic alloys,[22] but they are more striking for ceramics and have never been observed before.

(ii) Extrinsic dislocations seem to be generated from intergranular sources (Fig. 6), whereas in metals they are more likely to result from the interaction between lattice dislocations and grain boundaries. This may be expected because the flow stress required to activate Frank Read sources within grains is too elevated.[23] Grain boundaries appear as the possible sources for lattice dislocations in alumina polycrystals but, again, from this point of view, general grain boundaries are likely preferential sources.[24]

(iii) Lattice dislocations, rarely detected in previous TEM studies, have been observed in some small grains always bordered by a grain boundary containing dislocations (Fig. 7). The number of these grains increases with yttria codoping and, in that case, intragranular activity also includes stacking faults. Different 'lattice dislocation–grain boundary' configurations as shown in Fig. 8 have been investigated: in all cases, lattice dislocations are emitted by a general grain boundary, cross the small grain by a movement involving climb processes[25] and impinge on a special grain boundary in which they cannot be absorbed. Local reactions between lattice dislocations and intrinsic or extrinsic dislocations may exist (see Section 3.2), but total incorporation is impeded. In contrast, the latter process is likely to occur in general grain boundaries and may explain the absence of lattice dislocations in

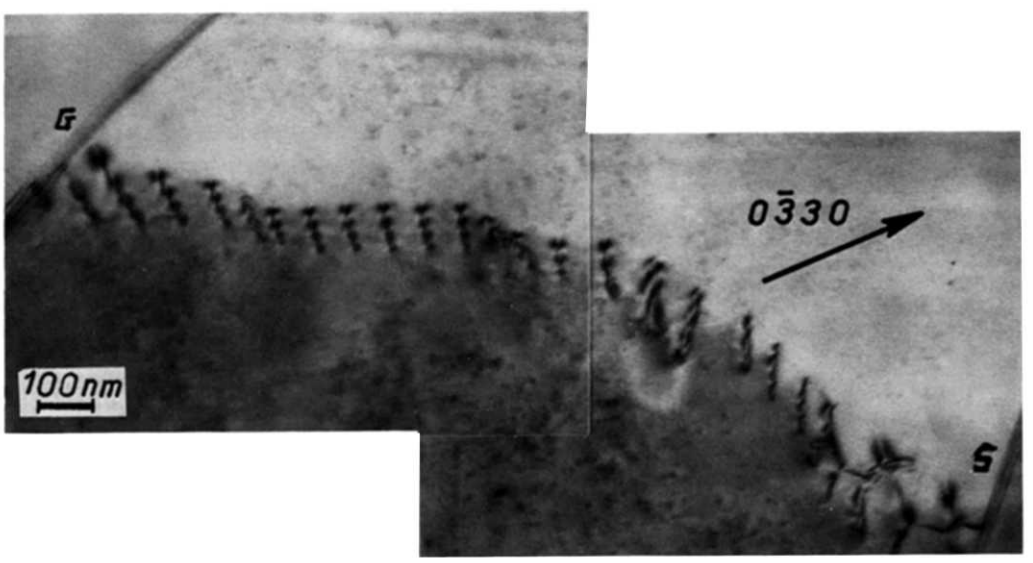

Fig. 8. Lattice dislocation array: dislocations emitted by the grain boundary G have a basal Burgers vector but are not in the basal slip plane indicating climb motion; their absorption is impeded in the special grain boundary S.

most grains of alumina polycrystals. General grain boundaries generate and absorb lattice dislocations, while near-coincidence grain boundaries cannot be either sources or sinks for lattice dislocations.

4.3 Grain boundary geometry and deformation

Near-coincidence grain boundaries (including low-angle (near $\Sigma = 1$), near one-dimensional coincidence and near-rational coincidence) are really 'special' grain boundaries in alumina as they display special behavior under high-temperature deformation.

'General' grain boundaries are favorable to superplasticity for two reasons:

—They are the paths along which grain boundary sliding may propagate.
—they allow the transfer of 'glide–climb' movement from one grain to another grain by absorption and emission of lattice dislocations.

'Special' grain boundaries appear as 'hard' elements of the microstructure; both grain boundary sliding and intragranular activity are impeded.

Intergranular segregation is able to influence the grain boundary behavior as is the case for yttrium, which plays a hardening role in the grain boundary accommodation processes.[25]

5 Grain Boundary Texture

This section has a double purpose:

(1) To investigate the possible contribution of grain boundaries to the overall creep deformation of doped alumina polycrystals, knowing that 'special' grain boundaries have a negative effect.

(2) To verify if the microstructure and ductility differences between doped and undoped aluminas are accompanied by differences in the grain boundary distributions in polycrystals (and possibly understand the reasons for such differences). Both the grain misorientation texture (Fig. 9) with reference to the previous geometric approach and the grain boundary plane texture (Fig. 10) have been determined for each type of polycrystal. Important differences appear between doped or codoped alumina and pure alumina.

After sintering, aluminas containing MgO or MgO and Y_2O_3 present a similar high proportion (35%) of 'special' grain boundary misorientations (this terminology includes low-angle (LA), one-dimensional coincidence (ODC) and three-dimensional near-coincidence (NC) grain boundaries). Pure aluminas display only 13% of one-dimensional coincidence grain boundaries (Fig. 9) (it is remarkable that no near three-dimensional coincidence grain boundaries occur in that case).

The proportions are inversed for the distributions of the grain boundary planes. Most of them are random in doped aluminas while 2/3 of them are dense planes of the structure in pure aluminas. In particular, basal planes seem to be favored (Fig. 10).

It must be underlined that a high proportion of near-coincidence grain boundaries is associated with a small grain size, and a high proportion of dense planes is associated with an exaggerated grain growth.

The selection of the basal plane for grain boundaries in alumina is not correlated to the presence of an amorphous phase; indeed, intergranular dislocations have been observed in some of these grain boundaries.

As a first conclusion, a near-coincidence misorientation and a dense grain boundary plane appear as two mutually exclusive criteria of grain boundary geometric speciality for alumina.

A high atomic density of the grain boundary plane

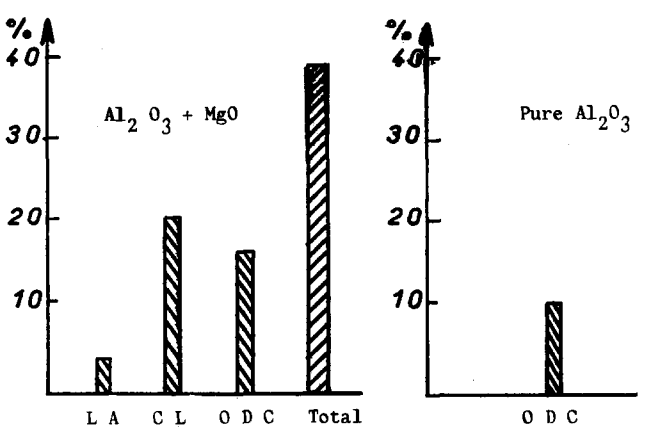

Fig. 9. Distribution of the grain misorientations in the Mg-doped and undoped aluminas (see text).

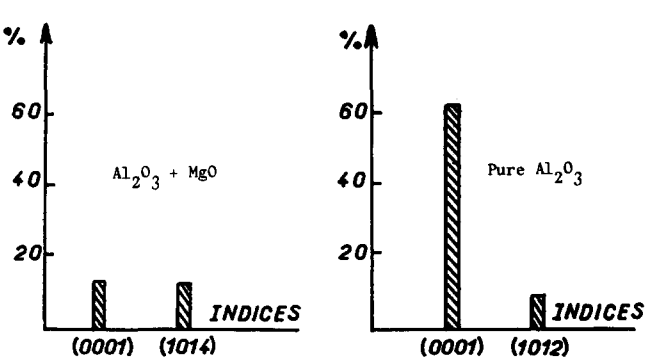

Fig. 10. Distribution of the grain boundary planes in the Mg-doped and undoped aluminas (see text).

appears a more restrictive parameter for creep deformation than a special misorientation (pure alumina cannot be compressed).

The different deformation behaviors of Mg-doped aluminas according to the presence or absence of yttria cannot be attributed to different proportions of near-coincidence grain boundaries but are probably due to a direct hardening effect of yttrium both on the grains and on the grain boundaries.

Finally, the high ductility of doped and codoped aluminas may be understood by taking into account their high proportion (65 to 70%) of general grain boundaries in which a set of accommodation processes involving diffusion called 'boundary dislocation creep'[20] may easily occur.

6 Conclusion

The analyses of a large number of grain boundaries in alumina polycrystals, made possible by the achievement of a theoretical method to describe coincidences in this rhombohedral and ionic oxide, present two main areas of interest:

—From a statistical point of view, the determination of the proportions of general and special grain boundaries is a prerequisite to understand the contribution of the intergranular microstructure to the overall deformation of polycrystals. Attempts at tailoring high-temperature deformation might be feasible via the control of grain boundary geometry distributions.

—From a fundamental point of view, all grain boundaries are submitted to the same high-temperature deformation mechanisms which are governed by the intergranular dislocation motion involving climb. Therefore, the 'boundary dislocation creep' processes are controlled by grain boundary diffusion and may be clearly revealed only in special boundaries where their kinetics are strongly decreased with respect to these kinetics in general grain boundaries. In this model, special grain boundaries appear to keep the memory of grain boundary phenomena.

Acknowledgements

The authors thank C. Carry of Ecole Polytechnique of Lausanne, Switzerland, who prepared the samples from highly pure powders and who performed sintering and compressive tests.

References

1. Fridez, J. D., Carry, C. & Mocellin, A., In *Advances in Ceramics, Vol. 10, Structure and Properties of MgO and Al_2O_3 Ceramics*, ed. W. D. Kingery. American Ceramic Society, Columbus, OH, 1985, pp. 720–40.
2. Carry, C. & Mocellin, A., *Proc. Brit. Ceram. Soc.*, **33** (1983) 101–15.
3. Bollmann, W., *Crystals Defects and Crystalline Interfaces*. Springer, Berlin, 1970.
4. Grimmer, H., *Acta Cryst.*, **A36** (1980) 382–9.
5. Grimmer, H., *Acta Cryst.*, **A45** (1989) 505–23.
6. Grimmer, H., *Helv. Phys. Acta*, **62** (1989) 231–40.
7. Priester, L., *Rev. Phys. App.*, **24** (1989) 419–38.
8. Grimmer, H., Bonnet, R., Lartigue, S. & Priester, L., *Phil. Mag.*, **A6** (1990) 493–509.
9. Bonnet, R. & Cousineau, E., *Acta Cryst.*, **A33** (1977) 850–6.
10. Lartigue, S. & Priester, L., *Acta Metall.*, **31** (1983) 1809–19.
11. Brandon, D. G., *Acta Metall.*, **14** (1966) 1479–84.
12. Pumphrey, P. H., *Scripta Metall.*, **6** (1972) 107–14.
13. Lartigue, S., Influence des dopants et de la déformation à chaud sur les paramètres cristallographiques des joints de grains et les dislocations intergranulaires dans l'alumine. Thesis, Université Paris-XI, Orsay, France, 1988.
14. Heuer, A. H. & Castaing, J., In *Advances in Ceramics, Vol. 10, Structure and Properties of MgO and Al_2O_3*, ed. W. D. Kingery. American Ceramic Society, Columbus, OH, 1985, pp. 238–57.
15. Chen, F. R. & King, A. H., *Phil. Mag.*, **A57** (1988) 431–55.
16. Bursill, L. A. & Withers, R. L., *Phil. Mag.*, **A40** (1979) 213–32.
17. Vicens, J., Laurent-Pinson, E., Chermant, J. L. & Nouet, G., *J. de Physique*, **C5-49** (1988) pp. 271–6.
18. Lartigue, S. & Priester, L., *J. de Physique*, **C5-49** (1988) 451–6.
19. Carry, C. & Mocellin, A., *Ceram. Int.*, **13** (1987) 89–98.
20. Dunlop, G. L. & Howell, P. R., In *Deformation of Polycrystals: Mechanisms and Microstructures*, ed. N. Hansen, A. Horsewell, T. Leffers & H. Lilholt, Risø, Denmark, 1981, pp. 261–9.
21. Lartigue, S. & Priester, L., *J. Amer. Ceram. Soc.*, **71**(6) (1988) 430–7.
22. Watanabe, T., *Res. Mechanica*, **11** (1984) 47–84.
23. Heuer, A. H., Tighe, J. N. & Cannon, R. M., *J. Amer. Ceram. Soc.*, **63**(1–2) (1980) 53–8.
24. Kurzydlowski, K. J., Varin, R. A. & Zielinski, W., *Acta Metall.*, **32** (1984) 71–79.
25. Lartigue, S., Carry, C. & Priester, L., *J. de Physique*, **C1-51** (1990) 985–90.